Manuscript submitted to
AIMS' Journals
Volume **X**, Number **0X**, XX **200X**

doi:10.3934/xx.xx.xx.xx

pp. **X–XX**

THE DYNAMICS OF PRINCIPAL SINGULAR CURVES: AN INNATE MOVING FRAME ON PARAMETRIC SURFACES

Moody Chu*

Department of Mathematics
North Carolina State University
Raleigh, North Carolina, 27695-8205, USA

Zhenyue Zhang

Department of Mathematics
Zhejiang University
Hangzhou, Zhejiang 310027, China

(Communicated by the associate editor name)

Abstract. This article reports an exploratory work that unveils some interesting yet unknown phenomena for all smooth functions over the Euclidean spaces. The findings are based on the fact that, generalizing the conventional gradient dynamics, the right singular vectors of the Jacobian matrix of any differentiable map point in directions that are most pertinent to the infinitesimal deformation of the underlying function and that the singular values measure the rate of deformation in the corresponding directions. A continuous adaption of these singular vectors therefore constitutes a natural moving frame that carries indwelling information of the variation. This inherence exists in functions over spaces of any dimensions, but the development of fundamental theory and algorithm for surface exploration is the important first step for immediate application and further generalization. For 2-parameter maps, including 3-D surfaces, trajectories of these singular vectors, referred to as singular curves, unveil some intriguing patterns per the given function. At points where singular values coalesce, curious and complex behavior occurs, manifesting specific landmarks for the function. Upon analyzing this dynamics, it is discovered that there is a remarkably simple and universal structure underneath all smooth 2-parameter maps. This work delineates with graphs this interesting dynamical system and the possibly new discovery that, analogous to the double helix with two base parings in DNA, two strands of critical curves and eight base pairings could encode properties of a generic and arbitrary surface. Such an innate structure thus arouses the curiosity, which is yet to be further investigated, that maybe this approach could lead to a unifying paradigm of function genetics where all smooth surfaces can be genome sequenced and classified accordingly.

2010 *Mathematics Subject Classification.* Primary: 37B35, 37N30, 65L07, 51N05, ; Secondary: 65D18, 53A05.

Key words and phrases. gradient adaption, singular curves, critical curves, base pairings, parametric surfaces, genome structure.

The first author is supported by the NSF grant DMS-1316779. The second author is supported by the NSFC project 11071218.

* Corresponding author: Moody Chu.

1. **Introduction.** The notion of nonlinear maps has been used in almost every field of disciplines as the most basic apparatus to describe complicated phenomena. However, the metaphysical question of what impinges on a function in such a way that we may make use of its variations to denote distinct episodes remain a natural mystery. Surface descriptions and their constructions in $\mathbb{R}^3$, for example, are of critical importance to a wide range of disciplines. But what makes surfaces to present so many different shapes and geometric properties? This paper reports a preliminary study of a dynamics system inbuilt in every function, which might suggest an alternative, interesting, and possibly universal paradigm to help explore these questions.

Our idea is motivated by the gradient adaption which is ubiquitous in nature. Heat transfer by conduction and osmosis of substances, moving respectively opposite to the temperature gradient which is perpendicular to the isothermal surfaces and down a concentration gradient across the cell membrane without requiring energy use, are just two common examples typifying this natural process. Gradient adaption follows the fundamental fact that the gradient

$$\nabla\eta(\mathbf{x}) := \left[\frac{\partial\eta}{\partial x_1}, \ldots, \frac{\partial\eta}{\partial x_n}\right]$$

of a given smooth scalar function $\eta : \mathbb{R}^n \longrightarrow \mathbb{R}$ points in the steepest ascent direction for the function value $\eta(\mathbf{x})$ with the maximum rate exactly equal to the Euclidean norm $\|\nabla\eta(\mathbf{x})\|$. A mechanical generalization of the gradient of a scalar function to a smooth vector function $\mathbf{f} : \mathbb{R}^n \longrightarrow \mathbb{R}^m$ should be the Jacobian matrix defined by

$$\mathbf{f}'(\mathbf{x}) := \begin{bmatrix} \frac{\partial f_1}{\partial x_1} & \cdots & \frac{\partial f_1}{\partial x_n} \\ \vdots & \ddots & \vdots \\ \frac{\partial f_m}{\partial x_1} & \cdots & \frac{\partial f_m}{\partial x_n} \end{bmatrix}.$$

In this situation, the information about how $\mathbf{f}(\mathbf{x})$ transforms itself is masked by the combined effect of m gradients. One way to quantify the variation of $\mathbf{f}$ is to measure the rate of change along any given unit vector $\mathbf{u}$ via the norm of the directional derivative

$$\lim_{t\to 0}\left\|\frac{\mathbf{f}(\mathbf{x}+t\mathbf{u})-\mathbf{f}(\mathbf{x})}{t}\right\| = \|\mathbf{f}'(\mathbf{x})\mathbf{u}\|. \tag{1}$$

Similar to the gradient adaption, we ask the question that along which directions the function $\mathbf{f}(\mathbf{x})$ changes most rapidly and how much the maximum rate is attained. The answer lies in the notion of singular value decomposition (SVD) of the Jacobian matrix $\mathbf{f}'(\mathbf{x})$.

Any given matrix $A \in \mathbb{R}^{m\times n}$ enjoys a factorization of the form

$$A = V\Sigma U^\top, \tag{2}$$

where $V \in \mathbb{R}^{m\times m}$ and $U \in \mathbb{R}^{n\times n}$ are orthogonal matrices, $\Sigma \in \mathbb{R}^{m\times n}$ is zero everywhere except for the nonnegative elements $\sigma_1 \geq \sigma_2 \geq \ldots \geq \sigma_\kappa > \sigma_{\kappa+1} = \ldots = 0$ along the leading diagonal, and $\kappa = \text{rank}(A)$. The scalars σ_i and the corresponding columns $\mathbf{u}_i$ in U and $\mathbf{v}_i$ in V are called the singular values, the right, and the left singular vectors of A, respectively [9]. The notion of the SVD has long been conceived in various disciplines [22] as it appears frequently in a remarkably wide range of important applications — data analysis [6], dimension reduction [16], signal processing [23], image compression, principal component analysis [24], to

name but a few. Among the multiple ways to characterize the SVD of a matrix A, the variational formulation,

$$\max_{\|\mathbf{u}\|=1} \|A\mathbf{u}\|, \tag{3}$$

sheds light on an important geometric property of the SVD. One can show that the unit stationary points $\mathbf{u}_i \in \mathbb{R}^n$ for problem (3) and the associated objective values $\|A\mathbf{u}_i\|$ are exactly the right singular vectors and the singular values of A. By duality, there exists a unit vector $\mathbf{v}_i \in \mathbb{R}^m$ such that $\mathbf{v}_i^\top A\mathbf{u}_i = \sigma_i$. This $\mathbf{v}_i$ is the corresponding left singular vector of A. Because the linear map A transforms the unit sphere in $\mathbb{R}^n$ into a hyperellipsoid in $\mathbb{R}^m$, the right singular vectors $\mathbf{u}_i$'s are the pivotal directions which are mapped to the semi-axis directions of the hyperellipsoid. Upon normalization, these semi-axis directions are precisely the left singular vectors $\mathbf{v}_i$'s. Additionally, the singular values measure the extent of deformation. In this way, it is thus understood that the SVD of the Jacobian matrix $\mathbf{f}'(\mathbf{x})$ carries crucial information about the infinitesimal deformation property of the nonlinear map $\mathbf{f}$ at $\mathbf{x}$. At every point $\mathbf{x} \in \mathbb{R}^n$, we now have in hand a set of orthonormal vectors pointing in particular directions pertinent to the variation of $\mathbf{f}$. These orthonormal vectors form a natural frame point by point.

It is often the case in nature that a system adapts itself continuously in the gradient direction. We thus are inspired to think that tracking down the "motion" of these frames might help reveal some innate peculiarities of the underlying function $\mathbf{f}$. More precisely, we are interested in the solution flows $\mathbf{x}_i(t) \in \mathbb{R}^n$ defined by the dynamical system

$$\dot{\mathbf{x}}_i \quad := \quad \pm\mathbf{u}_i(\mathbf{x}_i), \quad \mathbf{x}_i(0) = \widetilde{\mathbf{x}}, \tag{4}$$

or the corresponding solution flows $\mathbf{y}_i(t) \in \mathbb{R}^m$ defined by

$$\dot{\mathbf{y}}_i \quad := \quad \pm\sigma_i(\mathbf{x}_i)\mathbf{v}_i(\mathbf{x}_i), \quad \mathbf{y}_i(0) = f(\widetilde{\mathbf{x}}), \tag{5}$$

where $(\sigma_i, \mathbf{u}_i, \mathbf{v}_i)$ is the ith singular triplet of $\mathbf{f}'(\mathbf{x}_i)$. The scaling in (5) is to ensure the relationship

$$\mathbf{y}_i(t) = \mathbf{f}(\mathbf{x}_i(t)). \tag{6}$$

The sign $\pm$ in defining the vector field is meant to select the direction so as to avoid discontinuity jump because singular vectors are unique up to a sign change. Suppose $\dot{\mathbf{x}}(t) = \mathbf{u}(\mathbf{x}(t))$ and we define $\mathbf{z}(t) := \mathbf{x}(-t)$, then $\dot{\mathbf{z}}(t) = -\mathbf{u}(\mathbf{z}(t))$. We thus may assume, without loss of generality, that a direction of singular vectors has been predestined and that the time t can move either forward or backward.

It must be noted that any given point $\widetilde{\mathbf{x}}$ at which $\mathbf{f}'(\widetilde{\mathbf{x}})$ has at least one isolated singular vector cannot be an equilibrium point of the dynamical system (4). The frame therefore must move. What can happen is that the right side of (4) (or (5)) is not well defined at points when singular values coalesce because at such a point $\mathbf{f}'(\mathbf{x})$ has multiple singular vectors corresponding to the same singular value. A missed choice might cause $\dot{\mathbf{x}}_i$ (or $\dot{\mathbf{y}}_i$) to become discontinuous. We shall argue in this paper that it is precisely at these points that the nearby dynamics manifests significantly different behavior. Such a discontinuity is not to be confused with the theory of analytic singular value decomposition (ASVD) which asserts the existence of an analytic factorization for an analytic function in $\mathbf{x}$ [1, 25]. The subtle difference is that the ASVD guarantees an analytic decomposition as a whole without any ordering, but once we begin to pick out a specific singular vector, say, $\mathbf{u}_1(\mathbf{x})$ always denotes the right singular vector associated with the largest singular value σ_1, then $\mathbf{u}_1(\mathbf{x})$ by itself cannot guarantee its analyticity at the place where $\sigma_1 = \sigma_2$.

Because of the way they are constructed, the integral curves $\{\mathbf{x}_i(t)\}$ and $\{\mathbf{y}_i(t)\}$ are referred to in this paper as the right and the left *singular curves*[1] of the map $\mathbf{f}$, respectively. It suffices to consider only the right singular curves because the relationship (6) implies that their images under $\mathbf{f}$ are precisely the left singular curves. What makes this study interesting is that singular curves represent some curious undercurrents not recognized before of functions. Each function carries its own inherent flows. We conjecture that, under appropriate conditions, a given set of trajectories should also characterize a function. Exactly how such a correspondence between singular curves and a function take place remains an open question.

Singular curves do exist for smooth functions over spaces of arbitrary dimensions. However, singular vectors in high dimensional spaces generally do not have analytic form, making the analysis more challenging. In this paper, we study only the singular curves for 2-parameter functions so that we can actually visualize the dynamics. In particular, we focus on how it effects parametric surfaces in $\mathbb{R}^3$. Under this setting, it suffices to consider only the principal singular curves $\mathbf{x}_1(t)$ because the secondary singular curves $\mathbf{x}_2(t)$ are simply the orthogonal curves to $\mathbf{x}_1(t)$. Limiting ourselves to 2-parameter functions seems to have overly simplified the task. Nonetheless, we shall demonstrate that the corresponding dynamics already manifests some remarkably amazing exquisiteness.

The study of surfaces is a classic subject with long history and rich literature, both theoretically and practically. Research endeavors range from abstract theory in pure mathematics [2, 3, 20] to study of minimal surfaces [5, 18] and to applications in computer graphics, security, and medical images [4, 11, 12]. For instance, perhaps the best known classification theorem for surfaces is that any closed connected surface is homeomorphic to exactly one of the following surfaces: a sphere, a finite connected sum of tori, or a sphere with a finite number of disjoint discs removed and with crosscaps glued in their place [8]. To extract fine grains of surfaces, more sophisticated means have been developed. For example, the classic conformal geometry approach uses discrete Riemann mapping and Ricci flow for parametrization, matching, tracking, and identification for surfaces with arbitrary number of genuses [10, 11]. See also the work [21] where the notion of Laplace-Beltrami spectra is used as an isometry-invariant shape descriptor. We hasten to acknowledge that we do not have the expertise to elaborate substantially on these and other alternative methods for extracting geometric features of surfaces. Neither are we positioned to make a rigorous comparison. We simply want to mention that while these approaches for the geometry of surfaces are plausible, they might encounter three challenges – the associated numerical algorithms are usually complicated and expensive; the techniques designed for one particular problem are often structure dependent and might not be easily generalizable to another type of surface; and, most disappointedly, they could not offer to decipher what really causes a surface to behave in the way we expect it to behave. In contrast, our approach is at a much more rudimentary level than most of the studies in the literature. We concentrate on the dynamics of singular vectors that governs the structural dissimilarity of every smooth surface.

[1] The term "singular curve" has been used in different context in the literature. See, for example, [19]. We emphasize here its association with the singular value decomposition. Also, the notion of singular curves is fundamentally different from what is known as the principal curves used in statistics [7, 13, 14, 15].

Using the information-bearing singular value decomposition to study smooth nonlinear functions, which reveals a fascinating undercurrent per the given function, is perhaps the first of its kind. Our goal in this note therefore is aimed at merely conveying the point that the dynamical system of singular vectors dictates how a smooth function varies and vice versa. In particular, our initial investigation suggests a surprising and universal structure that is remarkably analogous to the biological DNA formation — associated with a general parametric surface in $\mathbb{R}^3$ are two strands of critical curves in $\mathbb{R}^2$ strung with a sequence of eight distinct base pairings whose folding and ordering might encode the behavior of a surface. A tantalizing new prospect thus comes this way — Would it be possible that a surface could be genome sequenced, synthesized, and its geometric properties be explained by the makeup of genes? This new subject is far from being completely understood. This work is only the first step by which we hope to stimulate some general interest.

This paper is organized as follows. For high dimensional problems, it is not possible to characterize the vector field (4) explicitly. For 2-parameter maps, we can describe the dynamical system in terms of two basic critical curves. These basics are outlined in Section 2. The intersection points of these critical curves are precisely where the dynamical system breaks down and, hence, contribute to the peculiar behavior of the system. In Section 3 we demonstrate the interesting behavior of the singular curves by a few parametric surfaces such as the Klein bottle, the Boy face, the snail and the breather surfaces. The first order local analysis of the dynamical system is given in Section 4. By bringing in the second order information in Section 5, we can further classify the local behavior in terms of base pairings which provide a universal structure underneath all generic parametric surfaces. In Section 6, we recast the singular vector dynamics over the classical scalar-valued functions and give a précis of how the notion of base pairing should be modified into "wedges" for this simple case. Finally, in Section 7 we outline a few potential applications, including a comparison with the gradient flows and a demonstration of the base pairing sequence.

2. Basics.

Given a differentiable 2-parameter function $\mathbf{f} : \mathbb{R}^2 \to \mathbb{R}^m$, denote the two columns of its $m \times 2$ Jacobian matrix by

$$\mathbf{f}'(\mathbf{x}) = \left[\ \mathbf{a}_1(\mathbf{x}),\, \mathbf{a}_2(\mathbf{x})\ \right].$$

Define the two scalar functions

$$\left\{ \begin{array}{rcl} n(\mathbf{x}) & := & \|\mathbf{a}_2(\mathbf{x})\|^2 - \|\mathbf{a}_1(\mathbf{x})\|^2 \\ o(\mathbf{x}) & := & 2\mathbf{a}_1(\mathbf{x})^\top \mathbf{a}_2(\mathbf{x}) \end{array} \right. \tag{7}$$

which measure, respectively, the disparity of norms and nearness of orthogonality between the column vectors of $\mathbf{f}'(\mathbf{x})$. Generically, each of the two sets defined by

$$\left\{ \begin{array}{rcl} \mathcal{N} & := & \{\mathbf{x} \in \mathbb{R}^n \,|\, n(\mathbf{x}) = 0\} \\ \mathcal{O} & := & \{\mathbf{x} \in \mathbb{R}^n \,|\, o(\mathbf{x}) = 0\} \end{array} \right. \tag{8}$$

forms a 1-dimensional manifold in $\mathbb{R}^2$ which is possibly empty or composed of multiple curves or loops. They will be shown in our analysis to play the role of "polynucleotide" connecting a string of interesting points and characterizing certain properties of a function.

A direct computation shows that the two singular values of $\mathbf{f}'(\mathbf{x})$ are given by

$$\begin{cases} \sigma_1(\mathbf{x}) &:= \left(\frac{1}{2}\left(\|\mathbf{a}_1(\mathbf{x})\|^2 + \|\mathbf{a}_2(\mathbf{x})\|^2 + \sqrt{o(\mathbf{x})^2 + n(\mathbf{x})^2}\right)\right)^{1/2}, \\ \sigma_2(\mathbf{x}) &:= \left(\frac{1}{2}\left(\|\mathbf{a}_1(\mathbf{x})\|^2 + \|\mathbf{a}_2(\mathbf{x})\|^2 - \sqrt{o(\mathbf{x})^2 + n(\mathbf{x})^2}\right)\right)^{1/2}. \end{cases} \tag{9}$$

The corresponding right singular vectors[2] are

$$\mathbf{u}_1(\mathbf{x}) := \frac{\pm 1}{\sqrt{1+\omega(\mathbf{x})^2}} \begin{bmatrix} \omega(\mathbf{x}) \\ 1 \end{bmatrix}, \tag{10}$$

$$\mathbf{u}_2(\mathbf{x}) := \frac{\pm 1}{\sqrt{1+\zeta(\mathbf{x})^2}} \begin{bmatrix} \zeta(\mathbf{x}) \\ 1 \end{bmatrix}, \tag{11}$$

respectively, where

$$\begin{cases} \omega(\mathbf{x}) &:= \frac{o(\mathbf{x})}{n(\mathbf{x})+\sqrt{o(\mathbf{x})^2+n(\mathbf{x})^2}}, \\ \zeta(\mathbf{x}) &:= \frac{-n(\mathbf{x})-\sqrt{o(\mathbf{x})^2+n(\mathbf{x})^2}}{o(\mathbf{x})}. \end{cases} \tag{12}$$

In the above, we normalize the second entry of the singular vectors with the understanding of taking limits when either $\omega(\mathbf{x})$ or $\zeta(\mathbf{x})$ becomes infinity. The following fact is observed immediately from (10).

Lemma 2.1. *The tangent vectors to the singular curves $\mathbf{x}_1(t)$ at any points in $\mathcal{N}$ but not in $\mathcal{O}$ are always parallel to either $\boldsymbol{\alpha}_n := \frac{1}{\sqrt{2}}[1,\,1]^\top$ or $\boldsymbol{\beta}_n := [1,\,-1]^\top$, depending on whether $o(\mathbf{x})$ is positive or negative. Likewise, the tangent vectors of the singular curves at any points in $\mathcal{O}$ but not in $\mathcal{N}$ are parallel to $\boldsymbol{\alpha}_o := [0,\,1]^\top$ or $\boldsymbol{\beta}_o := [1,\,0]^\top$, depending on whether $n(\mathbf{x})$ is positive or negative.*

At places where $\mathcal{N}$ and $\mathcal{O}$ intersect, which will be called *singular points*, the singular values coalesce and the (right) singular vectors become ambiguous. We shall argue that it is the angles of intersection by $\mathcal{N}$ and $\mathcal{O}$ at the singular point that affect the intriguing dynamics. The 1-dimensional manifolds $\mathcal{N}$ and $\mathcal{O}$ can be thought of as stringing singular points together (with particular pairings) and will be referred to as the *critical curves* of $\mathbf{f}$.

Example 1. It might be illustrative to plot the above basic curves by considering one graphic example $\mathbf{f} : \mathbb{R}^2 \to \mathbb{R}^2$ defined by

$$\mathbf{f}(x_1, x_2) := \begin{bmatrix} \sin(x_1 + x_2) + \cos(x_2) - 1 \\ \cos(2\,x_1) + \sin(x_2) - 1 \end{bmatrix}.$$

Applying a high-precision numerical ODE integrator to the differential system (4) at a mesh of starting points over the window $[-5,5]\times[-5,5]$, we find its singular curves $\mathbf{x}_1(t)$ behave like those in the left drawing of Figure 1, whereas its critical curves are sketched in the middle drawing. By overlaying the two drawings in the right graph of Figure 1, we can catch a glimpse into how these critical curves affect the dynamics of singular curves. In particular, the singular curves $\mathbf{x}_1(t)$ make interest twists nearby by points where $\mathcal{N}$ and $\mathcal{O}$ intersect. Also, take notice of the angles when the singular curves cut across the critical curves according to Lemma 2.1. Details will be analyzed in the sequel. In this example, note also that there are

[2]Expressions for both $\mathbf{u}_1$ and $\mathbf{u}_2$ are given, but we will carry out the analysis for $\mathbf{x}_1(t)$ only as that for $\mathbf{x}_2(t)$ can be done similarly. Also, $\mathbf{x}_2(t)$ is simply the orthogonal curve of $\mathbf{x}_1(t)$ in $\mathbb{R}^2$.

regions where the critical curves are extremely close to each other, forming long and narrow ridges with $\sigma_2/\sigma_1 > 0.95$.

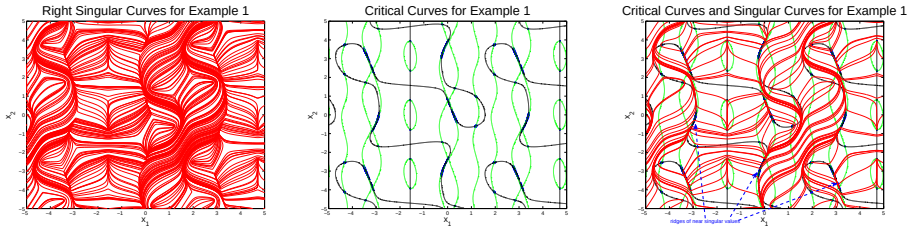

FIGURE 1. Example of singular curves (red) and critical curves: $\mathcal{N}$ (green); $\mathcal{O}$ (black).

3. **Application to parametric surfaces.** In this section we further demonstrate the critical curves, singular points, and the trajectories of (left) singular curves of a few selected parametric surfaces[3]. In all case, we denote the 2-parameter map in the form $\mathbf{f}(x_1, x_2) = (X(x_1, x_2), Y(x_1, x_2), Z(x_1, x_2))$ whose component are abbreviated as (X, Y, Z). Our point is that the surfaces might be complicated in $\mathbb{R}^3$, but the dynamics of the (right) singular curves could be surprisingly simple in $\mathbb{R}^2$.

Example 2. (Klein Bottle) With the abbreviations $c_1 := \cos x_1$, $s_1 := \sin x_1$, $c_2 := \cos x_2$, and $s_2 := \sin x_2$ for $x_1 \in [-\pi, \pi]$ and $x_2 \in [-\pi, \pi]$, the parametric equations

$$\begin{cases} X &:= -\frac{2}{15}c_1(3c_2 + 5s_1c_2c_1 - 30s_1 - 60s_1c_1^6 + 90s_1c_1^4) \\ Y &:= -\frac{1}{15}s_1(80c_2c_1^7s_1 + 48c_2c_1^6 - 80c_2c_1^5s_1 - 48c_2c_1^4 - 5c_2c_1^3s_1 - 3c_2c_1^2 \\ &\quad +5s_1c_2c_1 + 3c_2 - 60s_1) \\ Z &:= \frac{2}{15}s_2(3 + 5s_1c_1) \end{cases}$$

define a Klein bottle. In the left drawing of Figure 2, we find that critical curves for this particular Klein bottle are surprisingly simple. There is no $\mathcal{N}$ curve at all, whereas the $\mathcal{O}$ curves form vertical and horizontal grids. Therefore, there is no singular point in this case. We sketch two (right) singular curves by integrating the dynamics system (4) in both forward (red) and backward (blue) time from two distinct starting points[4] which are identifiable at the places where the colors are changed. It is interesting to note that in this example all right singular curves are horizontal, whereas their images, namely, the corresponding left singular curves, are periodic on the bottle and wind the bottle twice. The right drawing of Figure 2 is by removing the surface shown in the middle drawing.

[3]Admittedly, it is difficult to render a satisfactory 3-D drawing unless one can view the surface from different perspectives. The singular curves presented here are simply some snapshots of the far more complicated dynamics. We can furnish our Matlab code for readers to interactively play out the evolution of the singular curve at arbitrarily selected locations in $\mathbb{R}^2$. Also built in our code is a mechanism that can perform local analysis as we shall explain in the next section.

[4]The forward and backward directions of an integration are relative to the singular vector chosen at the starting point $\tilde{\mathbf{x}}$. Such a distinction is really immaterial. We mark them differently only to identify the starting point. If, however, the vector field $\mathbf{u}_1(\mathbf{x})$ is obtained through numerical calculation, then we must be aware that a general-purpose SVD solver cannot guarantee the continuity of $\mathbf{u}_1(\mathbf{x}(t))$, even if $\mathbf{x}(t)$ is continuous in t. An additional mechanism must be made to ensure that $\mathbf{u}_1(\mathbf{x}(t))$ does not abruptly reverse its direction, once the initial direction is set.

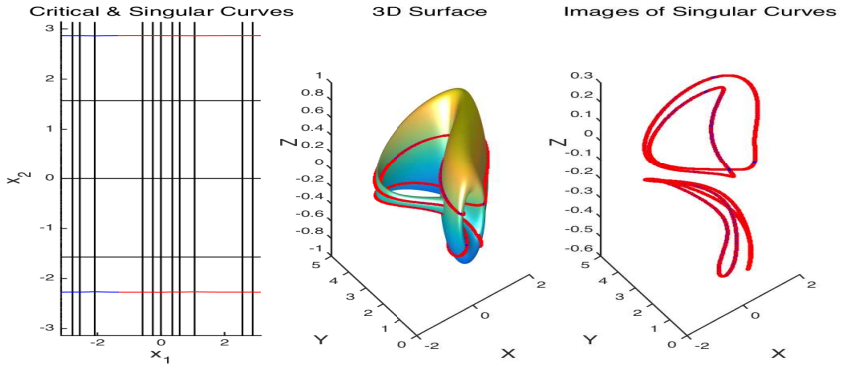

FIGURE 2. Klein bottle: $\mathcal{N}$ (green); $\mathcal{O}$ (black); singular curves (forward time (red); backward time (blue)).

If we perturb the equation by modifying some coefficients, the resulting surface is topologically equivalent to the original bottle. However, the critical curves are very different. The drawing of Figure 3 is the flattened bottle where the Y component is scaled down to 10% of its original value, i.e., the coefficient $-\frac{1}{15}$ is changed to $-\frac{1}{150}$. Note that now there are $\mathcal{N}$ curves and singular points and that the left singular curves are no longer periodic. We prefer to see this kind of distinction because it shows the idiosyncrasies even among topologically equivalent surfaces .

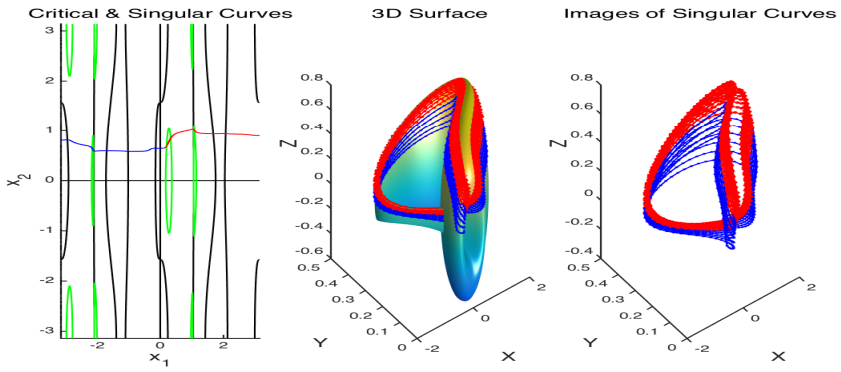

FIGURE 3. Klein bottle with Y down scaled: $\mathcal{N}$ (green); $\mathcal{O}$ (black); singular curves (forward time (red); backward time (blue)).

Example 3. (Boy's Surface) Denote $p := \cos x_1 \sin x_2$, $q := \sin x_1 \sin x_2$, and $r := \cos x_2$ for $x_1 \in [0, \pi]$ and $x_2 \in [0, 2\pi]$. Then the parametric equations

$$\begin{cases} X &:=: \ (2p^2 - q^2 - r^2 + 2qr(q^2 - r^2) + rp(p^2 - r^2) + pq(q^2 - p^2)) \\ Y &:= \ \frac{\sqrt{3}}{2}(q^2 - r^2 + (rp(r^2 - p^2) + pq(q^2 - p^2))) \\ Z &:= \ (p + q + r)((p + q + r)^3 + 4(q - p)(r - q)(p - r)). \end{cases}$$

define a Boy's face [17]. Shown in the left drawing of Figure 4, the critical curves repeat themselves as jigsaw puzzles with period π in both x_1 and x_2 directions and there are many singular points in this case. We integrate one right singular curve

starting at the location $(1, 4.5)$ over the extended domain in the x_2 direction to show how far it can migrate. A total of four singular points are involved. Going southwest, the forward time (red) integration passes by, but never touches, the first singular point A. Then it makes a U turn around a second singular point B and comes to a stop (due to the discontinuity) at a third singular point C. The backward time (blue) integration moves northeast, makes a U turn around a forth singular points D before it stops at the first singular point A. It is interesting to note that the first point A serves both as a roundabout and an attractor and that the fourth singular point is a translation by π of the second singular point. We rotate the XY-plane by 90° to show the back side of the (left) singular curves in the right drawing of Figure 4. As the Boy's surface is known to have no cuspidal points, an interesting question that is yet to be understood is the geometric significance of these singular points on the surface.

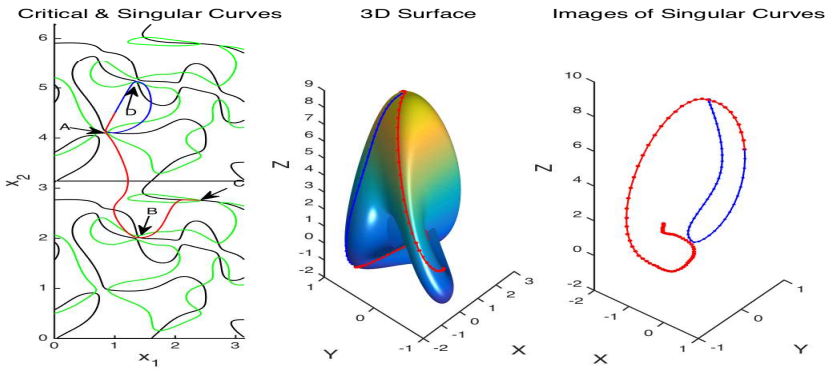

FIGURE 4. Boy's surface: $\mathcal{N}$ (green); $\mathcal{O}$ (black); singular curves (forward time (red); backward time (blue)).

Example 4. (Snail) Denote $v := x_2 + \frac{(x_2-2)^2}{16}$, $s := e^{-\frac{1}{10v}}$, and $r := s + \frac{7}{5} s \cos x_1$ for $x_1 \in [0, 2\pi]$ and $x_2 \in [-10, 35]$. Then the parametric equations

$$\begin{cases} X &:= r \cos v, \\ Y &:= 4(1-s) + \frac{7}{5} s \sin x_1, \\ Z &:= r \sin v \end{cases}$$

define a snail shape surface in $\mathbb{R}^3$. Despite the impression that the snail surface appears complicated, its critical curves are surprisingly simple. The left drawing in Figure 5 shows the $\mathcal{O}$ curves are straight lines intersecting the $\mathcal{N}$ curve at only two singular points in the given window. Not shown is the mirror image of the $\mathcal{N}$ curve with respect to the horizontal $\mathcal{O}$ curve, which produces exactly the same dynamics. In the left drawing of Figure 5, we integrate the right singular curve $\mathbf{x}_1(t)$ from one particular starting point (at where colors change). The forward (red) integration approaches asymptotically to the vertical $\mathcal{O}$ curve. The corresponding left singular curve converges to the tip of the snail. The backward (blue) integration converges to a singular point which indicates an "isotropic point" on the surface at which rates of change are identical in all directions. The snail does have a core inside the shell. The left singular curve curve plotted in the right drawing of Figure 5 traces that core.

In Figure 6 we cut open the snail by restricting $x_2 \in [-3, 3]$ to demonstrates another singular curve starting from $(2, -2)$. Note that its backward (blue) integration stays on the outside shell and converges to the tip of the snail while its forward (red) integration loops around the opening mouth of the snail.

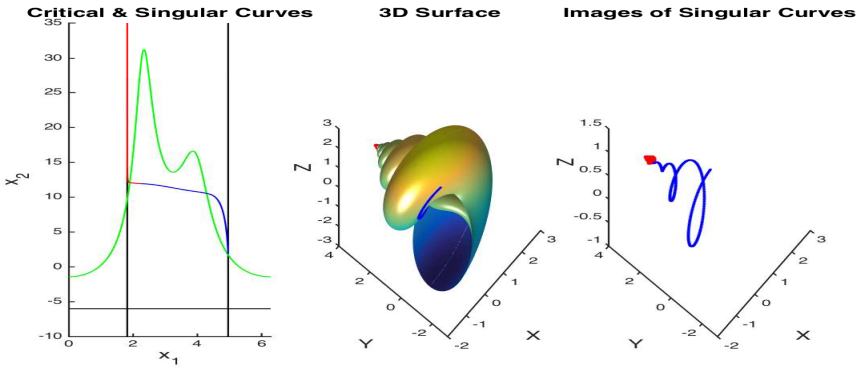

FIGURE 5. Snail: $\mathcal{N}$ (green); $\mathcal{O}$ (black); singular curves (forward time (red); backward time (blue)).

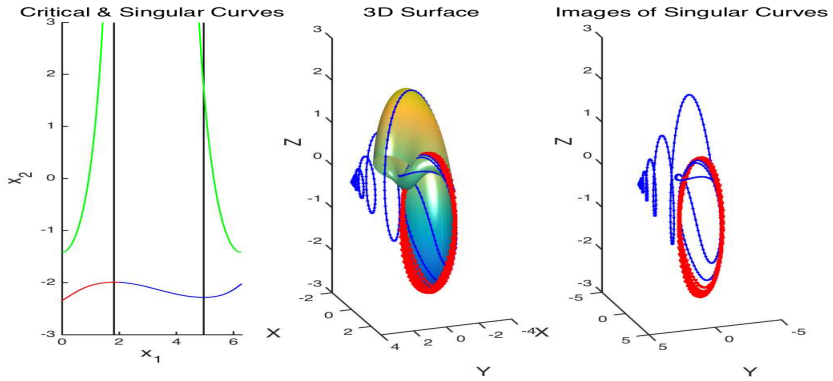

FIGURE 6. Snail: $\mathcal{N}$ (green); $\mathcal{O}$ (black); singular curves (forward time (red); backward time (blue)).

Example 5. (Breather) Denote $w := \frac{\sqrt{21}}{5}$ and $\rho := \frac{2}{5}((w\cosh(\frac{2}{5}x_1))^2+(\frac{2}{5}\sin(wx_2))^2)$. The parametric equations

$$\begin{cases} X &:= -x_1 + \frac{2w^2}{\rho}\cosh(\frac{2}{5}x_1)\sin(\frac{2}{5}x_1), \\ Y &:= \frac{2w\cosh(\frac{2}{5}x_1)}{\rho}(-w\cos(x_2)\cos(wx_2) - \sin(x_2)\sin(wx_2)), \\ Z &:= \frac{2w\cosh(\frac{2}{5}x_1)}{\rho}(-w\sin(x_2)\cos(wx_2) + \cos(x_2)\sin(wx_2)) \end{cases}$$

define a Breather surface where x_1 controls how the far the tips extend outward and x_2 controls how far the girth goes around. Starting with 0, every increment of x_2 by $\frac{5}{2\sqrt{21}}\pi \approx 3.42776$ defines one "vertebra" with two layers of "patagium" extended to the tips for a total of 22 vertebrae around the girth. We plot a portion of the

surface with $x_1 \in [-5, 5]$ and $x_2 \in [-2, 5]$ and some singular curves in Figure 7. There are periodic left singular curves on the vertebra, so the color distinction of the trajectories becomes futile. The horizontal $\mathcal{O}$ curves at $x_2 = 0, \frac{5}{2\sqrt{21}}\pi$, and so on are invariant under the right singular curves dynamics (4) whose corresponding left singular curves are precisely those "ribs" on the Breather surface. Again, we find it interesting that critical curves and singular curves are simple when comparing to the entirety of the Breather surface.

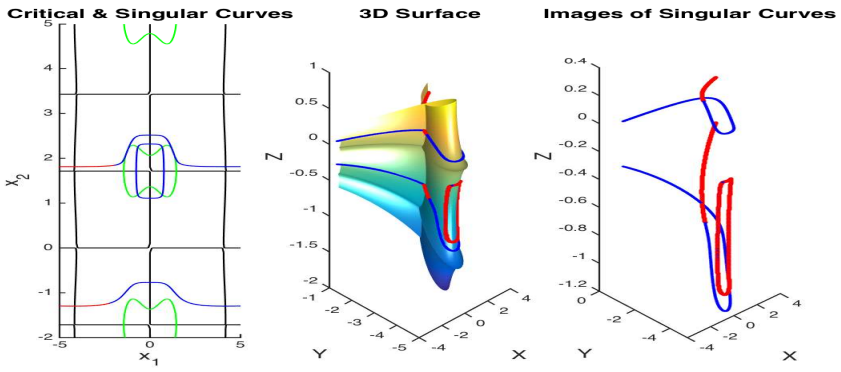

FIGURE 7. Breather: $\mathcal{N}$ (green); $\mathcal{O}$ (black); singular curves (forward time (red); backward time (blue)).

4. **Local Behavior.** We rewrite the dynamical system governing the (right) singular curves as

$$\dot{\mathbf{x}} = \pm \frac{1}{\sqrt{2\sqrt{n(\mathbf{x})^2 + o(\mathbf{x})^2}}} \begin{bmatrix} \frac{o(\mathbf{x})}{\sqrt{n(\mathbf{x}) + \sqrt{n(\mathbf{x})^2 + o(\mathbf{x})^2}}} \\ \sqrt{n(\mathbf{x}) + \sqrt{n(\mathbf{x})^2 + o(\mathbf{x})^2}} \end{bmatrix}, \tag{13}$$

which clearly shows that there are no equilibrium points, but becomes undefined at singular points. Let $\mathbf{x}_0$ be an isolated singular point. We now investigate the dynamical behavior nearby $\mathbf{x}_0$.

Consider the scenario where $\mathcal{N}$ and $\mathcal{O}$ intersect in the scheme depicted in Figure 8[5]. The short red segments denote tangent vectors of singular curves crossing the critical curves after taking into account the signs of $o(\mathbf{x})$ and $n(\mathbf{x})$. By Lemma 2.1, these directions are invariant on each halves of the critical curves. The portions of $\mathcal{N}$ and $\mathcal{O}$ where the tangent vectors of the crossing singular curves are parallel to the unit vectors $\boldsymbol{\alpha}_n = \frac{1}{\sqrt{2}}[1, 1]^\top$ and $\boldsymbol{\alpha}_o := [0, 1]^\top$, respectively, are referred to as the α-*halves* of the critical curves and denoted by n_α and o_α. Likewise, by changing α to β, we refer to the other halves of the critical curves. It is convenient to flag the critical curves by arrows to indicate the sides of n_α and o_α. In this generic case, the neighborhood of $\mathbf{x}_0$ is naturally divided into "quadrants" distinguished by the signs $(\mathrm{sgn}(n(\mathbf{x})), \mathrm{sgn}(o(\mathbf{x}))$ which, in a sense, imply a specific "orientation" of a local curvilinear coordinate system. With tangent vectors depicted in the left

[5]Here we have assumed the generic case where only one $\mathcal{N}$ curve and one $\mathcal{O}$ curve intersect at $\mathbf{x}_0$. It is possible that more then two critical curves are intersecting a singular point, e.g., the monkey saddle. To present the basic idea, we consider only the generic case here.

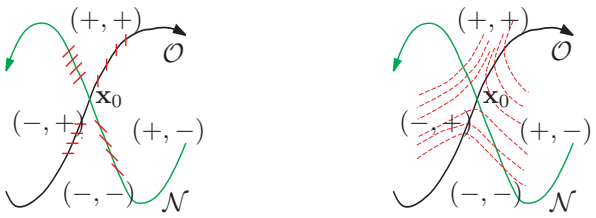

FIGURE 8. Local behavior nearby a propellent singular point $\mathbf{x}_0$.

drawing of Figure 8, the flow of the singular curves near $\mathbf{x}_0$ should move away from $\mathbf{x}_0$ as is depicted in the right diagram. In other words, the singular point $\mathbf{x}_0$ acts like a repeller for the flows $\mathbf{x}_1(t)$. If the orientation is switched such as that depicted in Figure 9, then the nearby dynamical behavior may change its topology.

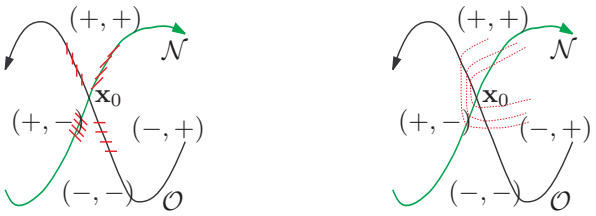

FIGURE 9. Local behavior nearby a roundabout singular point $\mathbf{x}_0$.

The manifolds $\mathcal{N}$ and $\mathcal{O}$ near $\mathbf{x}_0$ can be infinitesimally represented by their respective tangent vectors $\boldsymbol{\tau}_n$ and $\boldsymbol{\tau}_o$ at $\mathbf{x}_0$. Again we flag the originally undirected vectors $\boldsymbol{\tau}_n$ and $\boldsymbol{\tau}_o$ with arrows pointing to the corresponding α-halves of the critical curves. Starting with the north and centered at $\mathbf{x}_0$, divide the plane into eight sectors, each with a central angle $\frac{\pi}{4}$, and assign an ordinal number to name the sectors clockwise. The relative position of the two α-halves n_α and o_α with respect to these sectors is critical for deciding the local behavior. For easy reference, we say that we have the configuration (i, j) when $\boldsymbol{\tau}_n$ and $\boldsymbol{\tau}_o$ are located in the i-th and the j-th sectors, respectively. There are a total of 64 possible configurations.

Consider first the general case when $\boldsymbol{\tau}_n$ is not parallel to $\boldsymbol{\alpha}_n$ and $\boldsymbol{\tau}_o$ is not parallel to $\boldsymbol{\alpha}_o$. Special cases can be discussed in a similar manner. As already demonstrated earlier in Figures 8 and 9, the orientations of $\boldsymbol{\tau}_n$ and $\boldsymbol{\tau}_o$ do matter. The 48 configurations where $i \neq j$ and $|i - j| \neq 4$ already include $\boldsymbol{\tau}_n$ and $\boldsymbol{\tau}_o$ in reverse positions. Each of the 8 configurations where $i = j$ contains 2 distinct cases when the orientations of $\boldsymbol{\tau}_n$ and $\boldsymbol{\tau}_o$ are swapped. Likewise, each of the 8 configurations where $|i - j| = 4$ also contains 2 distinct orientations. Using the ideas described in Figures 8 and 9 to conduct an exhaustive search, we sketch all 80 possible local behaviors in Figure 10, some of which are identical by rotations. In all, we make the following observation.

Lemma 4.1. *Assume that a given singular point is the intersection of exactly one $\mathcal{N}$ curve and one $\mathcal{O}$ curve in its neighborhood. Assume also that at this point $\boldsymbol{\tau}_n$ is not parallel to $\boldsymbol{\alpha}_n$ and $\boldsymbol{\tau}_o$ is not parallel to $\boldsymbol{\alpha}_o$. Then the singular point serves to effect three essentially different dynamics, i.e., propellant, roundabout, or one-side roundabout and one-side attractor or propellant.*

The local bearings are identified by the two-letter marks, namely, the pairings, at the upper left corner in each case, which will be explained in the next section. We mention in passing that every even number column in the upper table in Figure 10 has the same paring as that in the odd column immediate to its left.

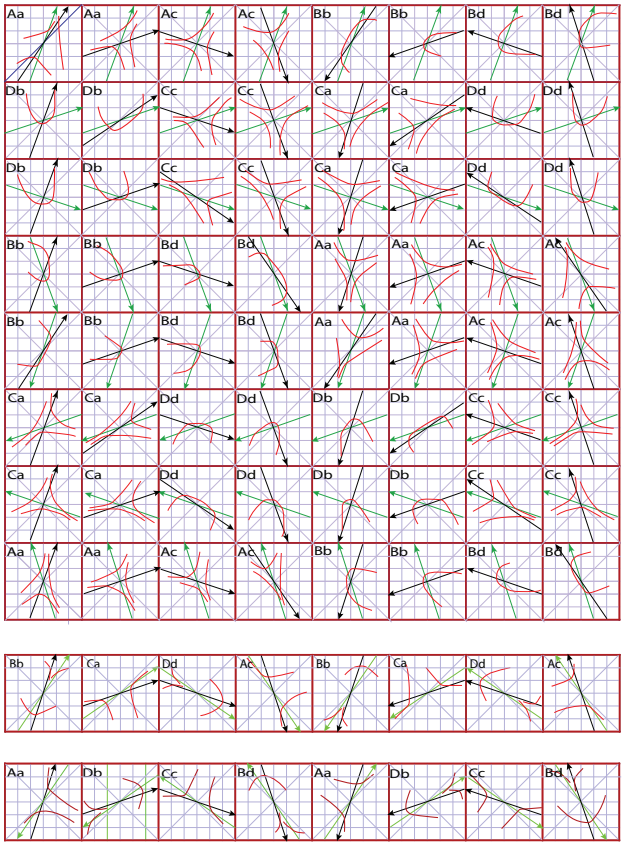

FIGURE 10. 80 possible local behaviors nearby a singular point $\mathbf{x}_0$. Arrows point at the α-halves n_α(green) and o_α (black).

5. **Base Pairing.** To justify the various curling behaviors of $\mathbf{x}_1(t)$ shown in Figure 10, we need to take into account more than just the first order derivative $\mathbf{u}_1(t)$. Observe that $\omega(\mathbf{x})$ can be expressed as

$$\omega(\mathbf{x}) := \begin{cases} \operatorname{sgn}\left(o(\mathbf{x})\right) - \frac{n(\mathbf{x})}{o(\mathbf{x})} + \frac{\operatorname{sgn}(o(\mathbf{x}))n(\mathbf{x})^2}{2o(\mathbf{x})^2} + O\left(n(\mathbf{x})^3\right), & \text{near } n(\mathbf{x}) = 0, \\ \frac{o(\mathbf{x})}{2n(\mathbf{x})} - \frac{o(\mathbf{x})^3}{8n(\mathbf{x})^3} + \frac{o(\mathbf{x})^5}{16n(\mathbf{x})^5} + O\left(o(\mathbf{x})^7\right), & \text{near } o(\mathbf{x}) = 0 \text{ and if } n(\mathbf{x}) > 0, \\ \frac{-1}{\frac{o(\mathbf{x})}{2n(\mathbf{x})} - \frac{o(\mathbf{x})^3}{8n(\mathbf{x})^3} + \frac{o(\mathbf{x})^5}{16n(\mathbf{x})^5} + O\left(o(\mathbf{x})^7\right)}, & \text{near } o(\mathbf{x}) = 0 \text{ and if } n(\mathbf{x}) < 0. \end{cases} \tag{14}$$

We already know that the first derivative of $\mathbf{x}_1(t)$ is related to $\omega(\mathbf{x}_1(t))$ via (10). The expansion (14) of $\omega(\mathbf{x})$ can now be used to estimate the second derivative of $\mathbf{x}_1(t)$.

In this way, we can characterize the concavity property and the local behaviors observed in Figure 10.

As an example, consider the case that we are at a point on n_α where the singular flow points necessarily in the direction $\boldsymbol{\alpha}_n$. Then it follows from (14) that the value of $\omega(\mathbf{x}(t))$ will increase if the vector $\mathbf{x}(t)$ moves to the side where $n(\mathbf{x}) < 0$, implying that the slope of the tangent vector $\mathbf{u}_1(\mathbf{x}(t))$ must be less than 1. Likewise, if $\mathbf{x}(t)$ moves to the side where $n(\mathbf{x}) > 0$, then the slope of $\mathbf{u}_1(\mathbf{x}(t))$ must be greater than 1. We therefore know how $\mathbf{x}(t)$ is bent.

A careful analysis concludes that, in all, near a singular point $\mathbf{x}_0$ and relative to a fixed $\boldsymbol{\tau}_n$ there are only four basic patterns, marked as A, B, C, and D, that the singular curves can cross the critical curve $\mathcal{N}$. Noting that $\boldsymbol{\tau}_n$ can be rotated to point in other directions, we sketch a few possible concavities of $\mathbf{x}_1(t)$ in Figure 11.

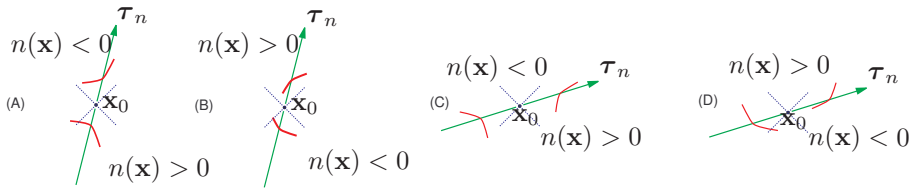

FIGURE 11. Basic concavities of singular curves near $n(\mathbf{x}) = 0$.

Similarly, suppose that we are at a point on o_α where the singular flow necessarily points in the direction of $\boldsymbol{\alpha}_0$. If the vector $\mathbf{x}(t)$ veers to the side where $\frac{o(\mathbf{x})}{n(\mathbf{x})} > 0$, then $\omega(\mathbf{x})$ increases from 0 and, hence, the absolute value of slop of the tangent vector $\mathbf{u}_1(\mathbf{x}(t))$ must decrease, causing the bend. Again, there are four basic concavities of $\mathbf{x}_1(t)$ marked as a, b, c, and d, near $\mathcal{O}$, subject to rotations, as depicted in Figure 12.

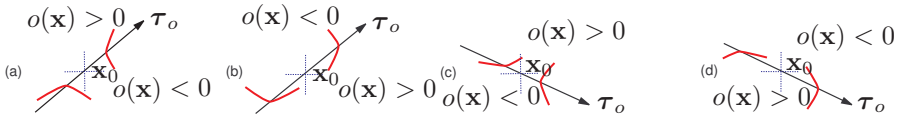

FIGURE 12. Basic concavities of singular curves near $o(\mathbf{x}) = 0$.

Paring the second order derivative information along both the $\mathcal{N}$ curve and the $\mathcal{O}$ curve does not give rise to 16 cases. Instead, after carefully examining the 80 possible dynamics in Figure 10, we make the following interesting observation.

Theorem 5.1. *Assume that a given singular point is the intersection of exactly one $\mathcal{N}$ curve and one $\mathcal{O}$ curve in its neighborhood. Assume also that at this point $\boldsymbol{\tau}_n$ is not parallel to $\boldsymbol{\alpha}_n$ and $\boldsymbol{\tau}_o$ is not parallel to $\boldsymbol{\alpha}_o$. Then the local behavior of the singular curves can be one of 8 possible patterns identified by the base parings Aa, Ac, Bb, Bd, Ca, Cc, Db, and Dd only. There is no other possible combinations.*

Proof. The result is nothing but from direct comparison case by case. More specifically, we have four ways of describing the concavity along the $\mathcal{N}$ curve near a singular point $\mathbf{x}_0$. These are the cases (A) and (C) where $\mathbf{x}_0$ behaves like a propellent and the cases (B) and (D) where $\mathbf{x}_0$ behaves like a roundabout. In the meantime, we have four similar ways of describing the concavity along the $\mathcal{O}$ curve.

Under the assumption, the case (A) or (C) can pair with (a) or (c) only to obtain a propellent. A pairing Ab or Ad is not possible because it will require the singular curve near $\mathbf{x}_0$ to have both a positive tangent and a negative tangent simultaneously. Likewise, the case (B) or (D) can pair with (b) or (d) only, whence $\mathbf{x}_0$ serves as either a roundabout or a mixture of one-sided roundabout and one-sided repellent/attractor. □

Each drawing in Figure 10 is identified by two letters of base paring at the upper left corner to indicate the corresponding dynamics. Each base paring has its own characteristic traits which can be distinguished by visualization, e.g., the difference between both Aa and Ac in configurations (1,2) and (1,3) are repellents but the difference is at whether the tailing is above or below $\boldsymbol{\beta}_o$. We shall not categorize the details as they might be too tedious to describe in this introduction paper. It is the combined effect of these basic curvatures which we refer to as *base pairing*, together with the positions of $\boldsymbol{\tau}_n$ and $\boldsymbol{\tau}_o$, that makes up the local dynamics observed in Figure 10. It is worth noting that a quick count shows that each base pairing results in 8 dynamics in the top drawing as general cases and 2 in the middle or bottom drawings as special cases. We shall characterize in Section 6 another situation under which different types of pairings might occur.

In the examples outlined in Section 3, there are cases not covered in Figure 10. Still, local behaviors of singular curves can be analyzed similarly, but need more details. One aspect is that they depend not only on the relative position of the tangent vectors $\boldsymbol{\tau}_o$ to $\boldsymbol{\tau}_n$ but also on which side of $\boldsymbol{\tau}_n$ that the α-half n_α resides. For instance, consider the scenario depicted in Figure 13 where that $\boldsymbol{\tau}_n$ points to the north-east and $\boldsymbol{\tau}_o$ is not parallel to $\boldsymbol{\tau}_n$, nor the east-west direction. Then there are 8 possible patterns. The subtlety is at the "crossover" of base pairings on the two sides of $\boldsymbol{\tau}_n$. In the two rightmost drawings of Figure 13, we observe that if n_α resides on the left side of $\boldsymbol{\tau}_n$, then we have the Bd dynamics similar to that of $(1, 8)$ in Figure 10; but if n_α veers to the right of $\boldsymbol{\tau}_n$, then we have the Dd dynamics similar to that of $(2, 8)$ in Figure 10. We denote this as a hybrid Bd/Dd base pairing which results in a roundabout behavior near the singular point $\mathbf{x}_0$ with distinct traits. Similarly, the Aa/Ca pairing results in a new type of repelling behavior near $\mathbf{x}_0$. Readers might try this out as an exercise for themselves. Without repeating mundane details, we mention that local patterns when $\boldsymbol{\tau}_o$ points in the north-south direction or even when $\boldsymbol{\tau}_n$ and $\boldsymbol{\tau}_o$ are parallel to each other can be explained by the idea outlined above.

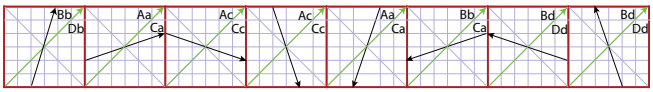

FIGURE 13. Relative positions of $\boldsymbol{\tau}_o$ and possible transitions of base pairings when $\boldsymbol{\tau}_n$ points to the north-east.

6. **Wedged bases of scalar-valued functions.** One simple but significant case must be mentioned because it commonly defies the assumption made in Theorem 5.1. Consider the surface that is the graph of a first-order continuously differentiable 2-variable function $f : \mathbb{R}^2 \to \mathbb{R}$. An obvious parametric equation is

$$\begin{cases} X &:= x_1 \\ Y &:= x_2 \\ Z &:= f(x_1, x_2). \end{cases} \tag{15}$$

It is easy to see that

$$\begin{cases} n(\mathbf{x}) &= \left(\frac{\partial f}{\partial x_2}\right)^2(\mathbf{x}) - \left(\frac{\partial f}{\partial x_1}\right)^2(\mathbf{x}), \\ o(\mathbf{x}) &= 2\frac{\partial f}{\partial x_1}(\mathbf{x})\frac{\partial f}{\partial x_2}(\mathbf{x}). \end{cases} \tag{16}$$

Thus a singular points $\mathbf{x}_0$ where $\mathcal{O}$ and $\mathcal{N}$ intersect must satisfy $\frac{\partial f}{\partial x_1}(\mathbf{x}_0) = \frac{\partial f}{\partial x_2}(\mathbf{x}_0) = 0$. In other words, the singular points are precisely the conventional critical points where the gradient of the function f vanishes. Indeed, we find from (10) that the first right singular vector is given by

$$\mathbf{u}_1 = \pm\left(1^2 + \left(\frac{n + \sqrt{n^2+o^2}}{o}\right)^2\right)^{-\frac{1}{2}} \begin{bmatrix} 1 \\ \frac{n+\sqrt{n^2+o^2}}{o} \end{bmatrix} = \pm\frac{1}{\sqrt{\frac{\partial f}{\partial x_1}^2 + \frac{\partial f}{\partial x_2}^2}} \begin{bmatrix} \frac{\partial f}{\partial x_1} \\ \frac{\partial f}{\partial x_2} \end{bmatrix}, \tag{17}$$

so the principal singular curve $\mathbf{x}_1(t)$ in the context of (15) is precisely the (normalized) gradient flow of $f(\mathbf{x})$. The choice of signs determines whether this is a descent flow or an ascent flow.

Furthermore, it is clear from (16) that $o(\mathbf{x})$ and $n(\mathbf{x})$ are always factorizable in this particular case. Define

$$\begin{cases} \mathcal{N}^1 &:= \{(x,y) | f_x(x,y) - f_y(x,y) = 0\}, \\ \mathcal{N}^2 &:= \{(x,y) | f_x(x,y) + f_y(x,y) = 0\}, \\ \mathcal{O}^1 &:= \{(x,y) | f_x(x,y) = 0\}, \\ \mathcal{O}^2 &:= \{(x,y) | f_y(x,y) = 0\}. \end{cases} \tag{18}$$

Each critical curve of either $\mathcal{O}$ or $\mathcal{N}$ has at least two separate components. So, at a singular point where all components meet together, there will be more than just two intersecting curves[6]. This situation is different from what we have detailed in Figure 10 and Theorem 5.1. The techniques employed earlier can readily be generalized to this case. However, the multiple components of critical curves allow more variations of sign changes for $n(\mathbf{x})$ and $o(\mathbf{x})$ near $\mathbf{x}_0$. It is possible to have multiple α-halves for $\mathcal{N}$ or $\mathcal{O}$ curves. The following result represents a typical case.

Lemma 6.1. *Assume that at a singular point $\mathbf{x}_0$ each of the curves defined in (18) contains exactly one curve. Then, up to the equivalence of rotations,*

1. *There are only four possible ways for singular curves to intersect with the $\mathcal{N}$ curve, as are shown Figure 14.*
2. *There are only four possible ways for singular curves to intersect with the $\mathcal{O}$ curve, as are shown in Figure 15.*

[6]For example, the function $f(x_1, x_2) = x_1^3 - 3x_1x_2^2$ has four components for each critical curve $\mathcal{O}$ or $\mathcal{N}$, so at the monkey saddle point a total of 8 critical curves intersect together.

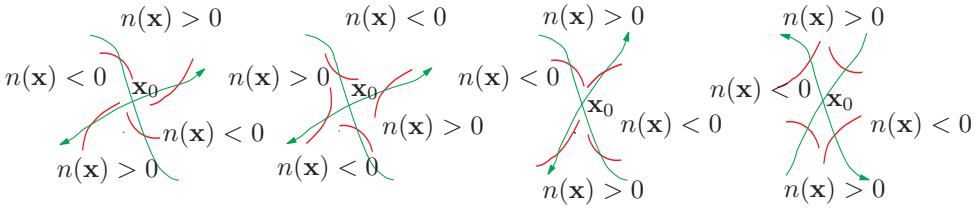

FIGURE 14. Basic concavities of singular curves near $n(\mathbf{x}) = 0$.

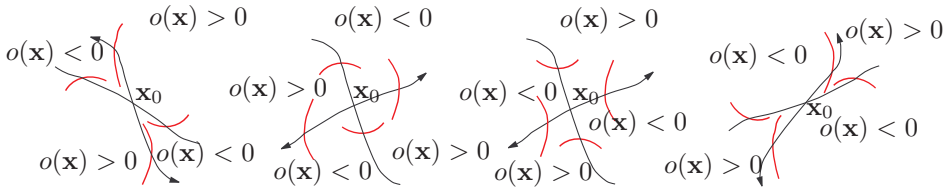

FIGURE 15. Basic concavities of singular curves near $o(\mathbf{x}) = 0$.

Proof. It can easily be checked that the singular curves cross the critical curves $\mathcal{N}^1, \mathcal{N}^2, \mathcal{O}^1$, and $\mathcal{O}^2$ with tangent vectors parallel to $\boldsymbol{\alpha}_n, \boldsymbol{\beta}_n, \boldsymbol{\alpha}_o$, and $\boldsymbol{\beta}_o$, respectively. Trivially, by (17), the tangent of the singular curve is $\frac{n+\sqrt{n^2+o^2}}{o}$. It follows that when a singular curve crosses the $\mathcal{N}$ curve, the absolute value of its tangent becomes greater than one when it enters the region $\{(x, y)|n(x, y) > 0\}$, and the absolute value of its tangent becomes less than one when it enters the region $\{(x, y)|n(x, y) < 0\}$. This property necessarily determines the concavity of the singular curves. The double-arrowed curve in Figure 14 represents $\mathcal{N}^1$. There can be only four positions of $\mathcal{N}^2$ relative to $\mathcal{N}^1$ that give rise to different local behaviors. Similarly, when a singular curve crosses the $\mathcal{O}$ curve, its tangent becomes positive when it enters the region $\{(x, y)|o(x, y) > 0\}$, and its tangent becomes negative when it enters the region $\{(x, y)|o(x, y) < 0\}$. □

Observe that in each of the eight basic drawings, the property of concavity is symmetric with respect to $\mathbf{x}_0$. Therefore, it suffices to identify the corresponding dynamics by simply the upper half wedge of each drawing. In this way, each wedge is still made of one α-half and one β-half with a cusp at $\mathbf{x}_0$. In Figure 11 and Figure 12, the concavity is determined by one single curve. In contrast, the concavities in the new bases are determined by two curves. These wedged bases give considerably more flexibility for pairing of $\mathcal{N}$ and $\mathcal{O}$. Indeed, we conjecture from our investigation that all 16 pairings are possible.

7. **Applications.** Thus far, we have been curious to study only the motifs of singular curves. The classification of all possible local behaviors suggests a simplistic collection of "tiles" for the delicate and complex "mosaics" observed in the dynamics of singular curves. The inherent characteristics of each given function determine the reflections or kinks of the critical curves $\mathcal{N}$ and $\mathcal{O}$ and a particular set of base pairings. These local tiles are strung together along the strands of critical curves to form the particular patterns of the underlying function. While there are zillions of possible variations, we find it interesting that there are only finitely many possible base pairings. To our knowledge, the dynamical system of singular curves has not

been studied before. The analysis on such a special differential system should be of theoretical interest in itself.

On the other hand, a successful exploration of the following two questions might help find important applications of the dynamical system of singular curves to parametric surfaces:

1. Given a parametric surface, can we decipher the making of its base pairings?
2. Given a sequence of base pairings together with a specific formation of critical curves, can we synthesize the main features of a surface?

At present, we are obviously far from complete understanding of these concepts. We are hoping that this paper will stimulate some further investigation from interested readers. For the idea to work, it seems plausible to expect that when a group of base pairings are strung together, they form a "gene" which, similar to the biological genes that dictate how the cells are going to live and function, should have the combine effect on determining how a surface would vary. We demonstrate two simple examples below.

Example 7. For surfaces arising in the form of (15), the singular points are the critical points and the singular curves are the gradient flows. As expected, the dynamics of singular curves therefore traces directions along which the function f changes most rapidly. On one hand, since we allow the integration to go in both forward and backward directions, every gradient trajectory stops at either a local maximum or a local minimum. Depending on the direction of the flows, these kinds of extreme points are either a sink or a source. In contrast to Lemma 4.1, these singular points are neither propellants nor roundabouts. On the other hand, the only other type of singular points are the saddle points of f around which the gradient (singular) trajectories will exhibit a mixture behavior. No Hessian information at the critical point is available unless we fix the sigh of the gradient. In all, we think we have enough knowledge to answer the above two questions almost in the same way as we learn to sketch a surface in multi-variable calculus.

Example 8. Critical curves $\mathcal{N}$ and $\mathcal{O}$ generally intertwine in a much more involved way. Once their α-halves are determined, which is precisely the inborn property of the underlying function, we begin to see the beauty and complexity of its mosaic patterns. We illustrate our point by color coding the the jigsaw pieces of Example 1 over a small window $[-2, 4] \times [-2, 4]$ in Figure 16 to evince the signs of $n(\mathbf{x})$ and $o(\mathbf{x})$. Singular points occurs at the common borders where the regions overlap, whose orientations are thus determined. We look up from Figure 10 to label the singular points with corresponding base pairings. We immediately notice that the same segment of the base parings, say, as short as BbAcBd in the drawing, determines almost the same dynamical behavior, and vise versa. The ideas about sequencing a surface or synthesizing a surface seems sensible.

Though we have all the local pieces in hand, we hasten to point out that there must be some other information missing in the current analysis of the dynamics. For instance, the two groups of singular curves near the point $(0, 1)$ in Figure 16 share the same Bd paring and, hence, local behavior. However, when away from this singular point, the singular curves wander off and are contracted to distinct destinations. This long term dynamics must have other bearings not explainable by our local analysis yet.

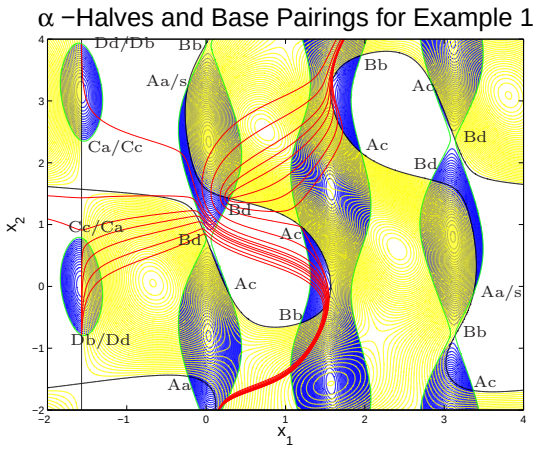

FIGURE 16. Base pairings for sample singular points in Example 1: $\mathcal{N}$ (green); $n(\mathbf{x}) > 0$ (blue); $\mathcal{O}$ (black); $o(\mathbf{x}) > 0$, (yellow).

8. **Conclusion.** Gradient adaption is an important mechanism occurring frequently in nature. Its generalization to Jacobian for vector functions does not reveal the critical adaption directions immediately. That information is manifested by the moving frame formed from the singular vectors of the Jacobian matrix. Intricate patterns resulting from singular curves seem to characterize some underneath movement of the function. The idea discussed in this paper is perhaps the first that relates the dynamical system of singular vectors to parametric surfaces.

The global behavior in general and its interpretation in specific of the dynamical system of singular vectors are yet to be completely understood. For parametric surfaces in $\mathbb{R}^3$ at least and for any $f : \mathbb{R}^2 \to \mathbb{R}^n$ in general, this work finds that two strands of curves joined by singular points with specific base pairings make up the local behavior of the function. In particular, at a singular point where exactly one $\mathcal{N}$ curve crosses exactly one $\mathcal{O}$ curve, there are exactly eight possible base pairings available.

This work aims at introducing the notion of singular curves. Many interesting questions remain to be answered, including whether a surface can be genome sequenced and synthesized.

REFERENCES

[1] A. Bunse-Gerstner, R. Byers, V. Mehrmann, and N. K. Nichols, *Numerical computation of an analytic singular value decomposition of a matrix valued function*, Numer. Math., 60 (1991), pp. 1–39.

[2] F. Cazals, J.-C. Faugère, M. Pouget, and F. Rouillier, *The implicit structure of ridges of a smooth parametric surface*, Comput. Aided Geom. Design, 23 (2006), pp. 582–598.

[3] S. S. Chern, *Curves and Surfaces in Euclidean space*, in Studies in Global Geometry and Analysis, Math. Assoc. Amer. (distributed by Prentice-Hall, Englewood Cliffs, N.J.), 1967, pp. 16–56.

[4] M. de Berg, O. Cheong, M. van Kreveld, and M. Overmars, *Computational geometry: Algorithms and applications*, Springer-Verlag, Berlin, third ed., 2008.

[5] U. Dierkes, S. Hildebrandt, and F. Sauvigny, *Minimal surfaces*, vol. 339 of Grundlehren der Mathematischen Wissenschaften [Fundamental Principles of Mathematical Sciences], Springer, Heidelberg, second ed., 2010.

[6] L. Eldén, *Matrix methods in data mining and pattern recognition*, vol. 4 of Fundamentals of Algorithms, Society for Industrial and Applied Mathematics (SIAM), Philadelphia, PA, 2007.
[7] D. Erdogmus and U. Ozertem, *Neural information processing*, Springer-Verlag, Berlin, Heidelberg, 2008, ch. Nonlinear Coordinate Unfolding Via Principal Curve Projections with Application to Nonlinear BSS, pp. 488–497.
[8] J. Gallier, *The Classification Theorem for Compact Surfaces And A Detour On Fractals*, University of Pennsylvania, 2005. available at http:\citeseerx.ist.psu.edu/viewdoc/download?doi=10.1.1.133.4358.
[9] G. H. Golub and C. F. Van Loan, *Matrix computations*, Johns Hopkins Studies in the Mathematical Sciences, Johns Hopkins University Press, Baltimore, MD, third ed., 1996.
[10] D. X. Gu, W. Zeng, L. M. Lui, F. Luo, and S.-T. Yau, *Recent development of computational conformal geometry*, in Fifth International Congress of Chinese Mathematicians. Part 1, 2, vol. 2 of AMS/IP Stud. Adv. Math., 51, pt. 1, Amer. Math. Soc., Providence, RI, 2012, pp. 515–560.
[11] X. D. Gu and S.-T. Yau, *Computational conformal geometry*, vol. 3 of Advanced Lectures in Mathematics (ALM), International Press, Somerville, MA, 2008.
[12] P. W. Hallinan, G. G. Gordon, A. L. Yuille, P. Giblin, and D. Mumford, *Two- and three-dimensional patterns of the face*, A K Peters, Ltd., Natick, MA, 1999.
[13] T. Hastie and W. Stuetzle, *Principal curves*, J. Amer. Statist. Assoc., 84 (1989), pp. 502–516.
[14] T. J. Hastie, *Principa Curves and Surfaces*, PhD thesis, Stanford University, available at http://www.slac.stanford.edu/pubs/slacreports/slac-r-276.html, 1984.
[15] B. Kégl, *Principal curves*, Université Paris Sud 11, available at http://www.iro.umontreal.ca/~kegl/research/pcurves/, 2012.
[16] V. C. Klema and A. J. Laub, *The singular value decomposition: its computation and some applications*, IEEE Trans. Automat. Control, 25 (1980), pp. 164–176.
[17] A. J. Maclean, *Parametric equations for surfaces*, University of Sydney, available at http://www.vtk.org/VTK/img/ParametricSurfaces.pdf, 2006.
[18] W. H. Meeks, III and J. Pérez, *The classical theory of minimal surfaces*, Bull. Amer. Math. Soc. (N.S.), 48 (2011), pp. 325–407.
[19] D. Mumford, *Curves and their Jacobians*, The University of Michigan Press, Ann Arbor, Mich., 1975.
[20] I. R. Porteous, *Geometric differentiation: For the intelligence of curves and surfaces*, Cambridge University Press, Cambridge, second ed., 2001.
[21] M. Reuter, F.-E. Wolter, and N. Peinecke, *Laplace-Beltrami spectra as "shape-DNA" of surfaces and solids*, Computer-Aided Design, 38 (2006), pp. 342–366. Symposium on Solid and Physical Modeling 2005.
[22] G. W. Stewart, *On the early history of the singular value decomposition*, SIAM Rev., 35 (1993), pp. 551–566.
[23] J. Vandewalle and B. De Moor, *On the use of the singular value decomposition in identification and signal processing*, in Numerical linear algebra, digital signal processing and parallel algorithms (Leuven, 1988), vol. 70 of NATO Adv. Sci. Inst. Ser. F Comput. Systems Sci., Springer, Berlin, 1991, pp. 321–360.
[24] M. E. Wall, A. Rechtsteiner, and L. M. Rocha, *Singular value decomposition and principal component analysis*, in A Practical Approach to Microarray Data Analysis, D. P. Berrar, W. Dubitzky, and M. Granzow, eds., Kluwer, Norwell, MA, available at http://www.springerlink.com/content/x035256j0h64h187/ ed., 2003, ch. 5, pp. 91–108.
[25] K. Wright, *Differential equations for the analytic singular value decomposition of a matrix*, Numer. Math., 63 (1992), pp. 283–295.

E-mail address: chu@math.ncsu.edu
E-mail address: zyzhang@zju.edu.cn